Femtosecond Photoelectron Imaging on Pyrazine: (1+2′) REMPI of Deuterated Pyrazine

Toshinori Suzuki*,‡ and Li Wang†

Institute for Molecular Science, Myodaiji, Okazaki 444-8585, Japan

Masaaki Tsubouchi‡

The Graduate University for Advanced Studies, Okazaki 444-8585, Japan

Received: March 31, 2004; In Final Form: April 29, 2004

Femtosecond time-resolved photoelectron imaging was applied to (1+2′) resonance-enhanced multiphoton ionization of deuterated pyrazine. The resonances with the 3s and 3p Rydberg states and rotational dephasing on a picosecond time-scale were observed similarly with pyrazine-H4. The photoionization dynamics of pyrazine-D4 was found to be identical to that of H4 at the photoionization wavelength of 393 nm. No signature was observed of the influence of the superexcited states upon ionization.

Introduction

Femtosecond time-resolved photoelectron imaging (TR-PEI) is a powerful experimental means to probe radiationless transitions in polyatomic molecules.[1,2] As ionization is allowed from any excited states with different multiplicities, there is essentially no dark state that cannot be observed, as far as the probe (ionization) laser wavelength is sufficiently short. This makes possible the study of intersystem crossing (ISC) in real time.[1,3−7]

In one-photon ionization from the excited state, the observed photoelectron kinetic energy distribution (PKED) becomes a Franck−Condon overlap, in the first-order approximation, between the nonstationary wave packet in the excited neutral state and the cationic state vibrational wave functions. This allows the examination of the vibrational dynamics in the neutral excited state.[8] This approach is, however, not always advantageous. When the photoexcited polyatomic molecule undergoes significant geometry change and, at the same time, electronic dephasing such as ISC or internal conversion (IC), the excited-state wave function spreads over a wide area of the multiple potential energy surfaces, causing the PKEDs due to ionization from different electronic states to overlap each other. This complexity is avoided by the use of (1+2′) ionization using the resonances with Rydberg states at the energy of $\hbar\omega_1 + \hbar\omega_2$ (Figure 1).[6,7,9] This is because ionization from the Rydberg state to the cation obeys the propensity rule of $\Delta v = 0$ due to the orthogonality of the vibrational wave functions. This makes each ionization channel appear as a single peak in PKED and greatly simplifies the observation of radiationless transitions by TR-PEI. In addition, the (1+2′) scheme is technically easier than the (1+1′) scheme, as the visible light does not induce background photoemission from the apparatus, which is sometimes problematic with the deep UV and VUV light.

In our previous paper, we have used (1+2′) TR-PEI to study S_1-T_1 ISC in pyrazine, the best-known intermediate coupling case in the molecular radiationless transition,[10] and we observed the formation of the T_1 states in real time.[4,6] From an extensive analysis of the PKEDs and the photoelectron angular distributions (PADs), resonances with the 3s and 3p Rydberg states at the $\hbar\omega_1 + \hbar\omega_2$ energy were identified in ionization from both singlet and triplet manifolds.[9] Clearly separated ionization signals from the singlet and triplet states allowed us to observe rotational wave packet dynamics in the bright and darks states separately for the first time.[6] We found that the molecular structure in the triplet state is quite similar to that in the singlet, while the strength of the molecular axis alignment significantly diminished in the triplet.[6] The reduction of the alignment was theoretically explained by an angular momentum coupling mechanism upon ISC.[11] TR-PEI also allowed the observation

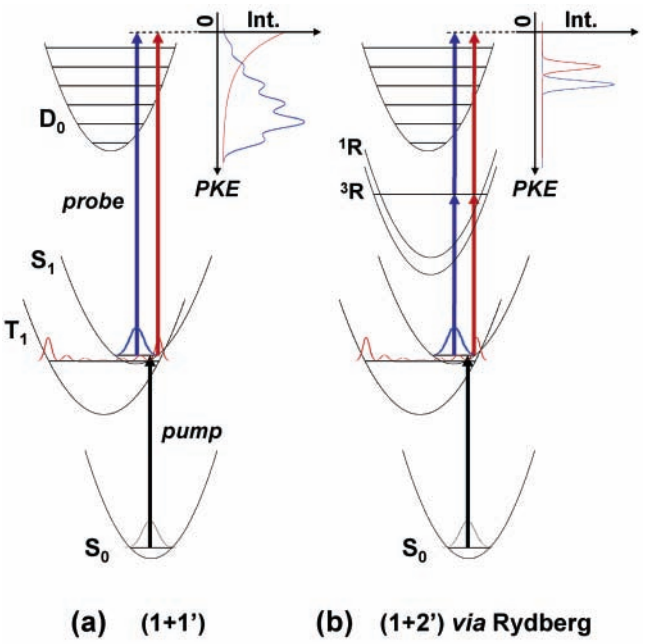

Figure 1. A schematic diagram of (a) (1+1′) and (b) (1+2′) REMPI where the second resonance enhancement occurs at $\hbar\omega_1 + \hbar\omega_2$ with the Rydberg states in the latter. The photoelectron energy peak becomes sharp because of the $\Delta v = 0$ propensity rule upon ionization from the Rydberg state to the ionization continuum.

* Corresponding author. E-mail: toshisuzuki@riken.jp.
† Present address: Dalian Institute of Chemical Physics, Chinese Academy of Sciences, China.
‡ Present address: Chemical Dynamics Laboratory, RIKEN, Wako, 351-0198, Japan.

10.1021/jp0486043 CCC: $27.50
Published on Web 06/12/2004

of PAD for an ensemble of molecules aligned by the pump laser light, with which ionization dynamics was examined in detail.

In this paper, we apply (1+2′) TR-PEI to deuterated analogue (pyrazine-D4) and compare the results with pyrazine-H4. In TR-PEI, it may often be assumed that the final state of ionization has rather simple wave functions of a cation core and a scattering outgoing wave of a photoelectron. This, however, has to be considered carefully as the superexcited neutral states are embedded in the continuum and they might affect ionization dynamics. One method to explore any effect of superexcited states upon ionization is to vary the ionization wavelength to examine on- and off-resonance with the metastable state. However, in our experimental scheme, the probe laser plays a dual role of excitation from the S_1 state to the Rydberg state and excitation from the Rydberg to the continuum. Therefore, this approach is not ideal in the present case, as the variation of the probe wavelength changes both the vibrational energy in the Rydberg state and the excess energy in the ionization continuum. Alternatively, we use deuterated sample to alter the vibrational wave functions while maintaining their symmetric properties and compare the ionization dynamics with that of pyrazine-H4 in the present work. The C−H oscillators have the largest influence on the Franck−Condon overlap in the vibronic coupling between different electronic states, and its deuteration effect has been extensively studied in molecular radiationless transitions. Therefore, it is interesting to compare the ionization dynamics of pyrazine-D4 and H4 with the same probe wavelength.

Experimental Section

A solid-state femtosecond laser system consists of a YVO_4-pumped Ti:sapphire oscillator (Spectra Physics Millennia and Tsunami) and a 10 Hz Nd:YAG-pumped Ti:sapphire regenerative amplifier (Spectra Physics GCR-190 and TSA-10). The output of the amplifier is split into two beams in which one beam is used to excite an optical parametric amplifier (Light Conversion Topas Deep-UV) to generate tunable UV pump pulse and the other is frequency-doubled in a BBO crystal to generate the second harmonic (393 nm) probe pulse. The pump and probe beams are aligned coaxially and are focused on the molecular beam with a lens $f = 450$ and 500 mm, respectively. The power densities of the pump and probe laser pulses at the interaction region were estimated to be less than 10^{10} and 5×10^{10} W/cm^2, respectively. The cross-correlation was ca. 450 fs.

Deuterated pyrazine 1% in He was prepared in a reservoir at room temperature and was expanded from a pulsed valve driven by a piezoelectric crystal with a stagnation pressure of 1.4 atm relative to the vacuum. The supersonic jet formed is collimated by a skimmer 0.8 mm in diameter in a source chamber evacuated by a 2000 L/s turbo molecular pump (Seiko Seiki STP2000) and introduced into the main chamber evacuated by a 500 L/s turbo molecular pump (Pfeiffer-Balzers TPU500). The molecular and laser beams are crossed inside of the electrodes for acceleration of photoelectrons.[12] The electrons fly through a field free region 44 cm in length that is magnetically shielded by a μ-metal tube. At the end of the flight tube, the electrons strike a dual microchannel plate backed by a P20 phosphor screen (Photek, OFD40), and the image on the screen is coupled out of the vacuum chamber using a fiber bundle.

The image that appears at the end of the fiber is captured with an image-intensified video-rate CCD camera (Hamamatsu ICCD, 768 × 572 pixels) and each video frame is transferred to a host computer on which image processing is performed on each video frame. The numerical processing includes thresholding to eliminate electrical noise and centroiding of light spots to enhance the image resolution to a single pixel size.[13] An inverse-Abel transform is used to calculate slices through the 3D scattering distributions of electrons from the observed 2D projection images. The time-delay between the pump and probe lasers is varied with a computer-controlled delay stage (Sigma-Koki Mark-12 and STM-160).

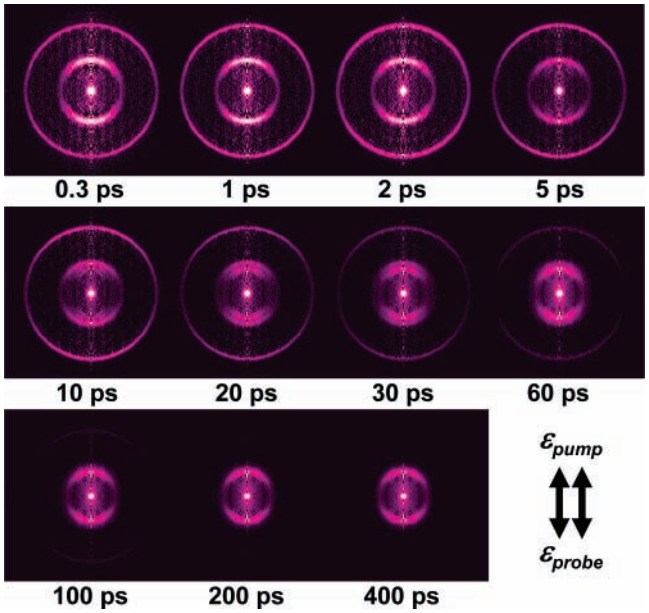

Figure 2. A series of time-resolved photoelectron images (inverse-Abel transform) of pyrazine-D4 observed with a pump laser wavelength of 322 nm at the 0_0^0 band of the S_1-S_0 transition of pyrazine-D4 and a probe wavelength of 393 nm. Raw images were integrated for 3.2×10^4 laser shots. The linear polarization of the pump and probe lasers is aligned vertical in the plane of the figure.

Results and Discussion

Figure 2 shows typical photoelectron images observed with the pump laser wavelength of 322 nm that is resonant with the 0_0^0 band of the $S_1(n,\pi^*)-S_0$ transition of pyrazine-D4. The images correspond to slices through the 3D photoelectron scattering distributions observed at quoted time-delays. The linear polarization of the pump and probe lasers is aligned vertical in the plane of the figure. These images consist of three rings in which the outer two rings appear at short pump−probe time-delays, whereas the innermost ring emerges at a later time. From the analogy with previous results on pyrazine-H4,[4−6,9] these rings are readily assigned to photoionization from the S_1 and T_1 manifolds via the resonances with the singlet 3s, the singlet $3p_z$, and the triplet 3s Rydberg states. The z axis is defined through the two nitrogen atoms.

Integration of the angular part of these images provides time-dependent PKEDs shown in Figure 3a. As seen here, each peak is quite sharp, confirming that ionization occurs via the Rydberg states for which the $\Delta v = 0$ vibrational propensity rule applies. The width of the peak is slightly wider for higher kinetic energy as the instrumental resolution is nearly constant over the photoelectron speed rather than the energy. The photoelectron kinetic energy, PKE, in (1+2′) REMPI via the resonance with the Rydberg state is provided by[9]

$$\mathrm{PKE} = T_\mathrm{R} + \hbar\omega_2 - \mathrm{IP} = \hbar\omega_2 - \frac{R}{(n-\delta)^2} \qquad (1)$$

where T_R is the term value of the Rydberg state, IP is the

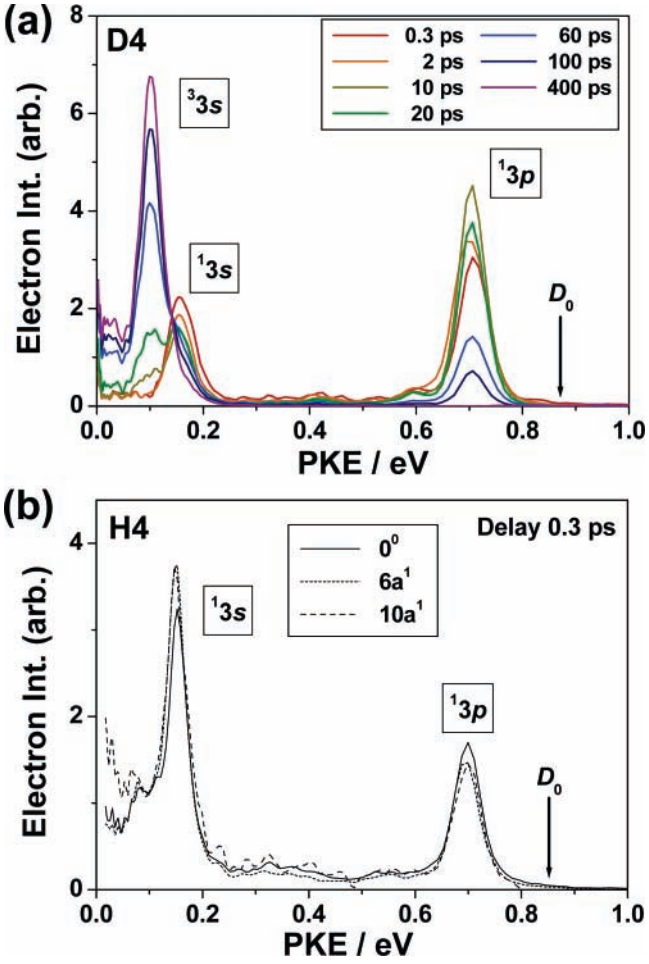

Figure 3. (a) Time-resolved photoelectron kinetic energy distributions (PKEDs) of pyrazine-D4 extracted from the images shown in Figure 2. These spectra were observed by (1+2′) REMPI via the S_1 0^0 state with 322 nm pump and 393 nm probe light. The photoelectron energy (870 meV) expected for ionization to the zero vibrational level of the cation is indicated by D_0. (b) PKEDs of pyrazine-H4 at the pump−probe time-delay of 0.3 ps. These spectra were observed by (1+2′) REMPI via the S_1 0^0, $10a^1$, and $6a^1$ vibronic states pumped by 323, 319, and 317 nm light, respectively. The probe light wavelength is 393 nm. D_0 is at 851 meV.

TABLE 1: Assignments of the Rydberg States of Pyrazine-D4

PKE/meV	assignment	E_{excess}[a]/cm^{-1}	T_R[b]/cm^{-1}	T_R[c]/cm^{-1}	δ
708	3p$_z$ ($^1B_{1u}$)	1310	55 170	55 288	0.64
159	3s (^1A_g)	5730	50 740		0.87
101	3s (^3A_g)	6200	50 270		0.89

[a] Excess energy of the (1+2′) REMPI with 322 nm pump and 393 nm probe light. [b] This work. [c] Reference 16.

ionization potential, R is the Rydberg constant, n is the principal quantum number of the Rydberg state, and δ is the quantum defect. The assignments of the Rydberg states are summarized in Table 1. As far as we know, the IP of pyrazine-D4 has not been measured. In the case of benzene, the difference in the IPs between D6 and H6 was observed to be $\Delta IP = 26.632$ cm^{-1} [ref 14] and is smaller than our energy resolution (>50 cm^{-1}). Therefore, in applying eq 1 to pyrazine-D4, we simply used the IP of pyrazine-H4, 74 903 cm^{-1} [ref 15]. The term value of the 3p$_z$ state (55 170 cm^{-1}) agrees well with the literature value of 55 288 cm^{-1} [ref 16]. Because of the inversion symmetry, the transition to the 3p state with ungerade symmetry from the S_1($^1B_{3u}$) state is forbidden, and it is only induced by vibronic couplings.

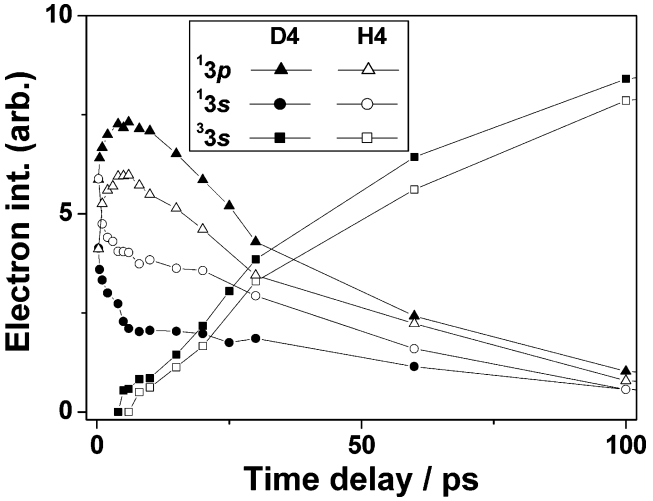

Figure 4. Temporal profiles of the energy selected photoelectron intensities of pyrazine-D4 and -H4. These were observed by (1+2′) REMPI via the S_1 0^0 state.

For comparison, Figure 3b shows similar results obtained for pyrazine-H4 at the pump−probe time-delay of 0.3 ps. These spectra were observed by (1+2′) REMPI via the S_1 0^0, $10a^1$, and $6a^1$ vibronic levels pumped at 323, 319, and 317 nm, respectively. Close comparison reveals that the intensity ratios of the singlet 3s and 3p$_z$ peaks are different between H4 and D4: the 3s peak is much stronger than 3p$_z$ in H4, while it is not in D4. The result may be explained by the fact that excitation to the 3s state reaches highly excited vibrational levels with E_{excess} listed in Table 1 and the Franck−Condon factor with a zero vibrational level of S_1 is smaller in D4 than in H4. An alternative explanation is that excitation to the 3p$_z$ state occurs to its relatively low vibrational levels and the overlap of the probe laser wavelength with the discrete band structure changes the peak intensity of 3p$_z$ in the PKEDs of H4 and D4. As seen in Figure 3b, the PKED observed with (1+2′) REMPI does not vary with the vibrational energy in the S_1 state. When the pump laser wavelength is varied in this (1+2′) REMPI scheme, the vibrational energy in the Rydberg state varies, as the probe laser wavelength is fixed. Nevertheless, the PKED stays identical, proving the validity of eq 1.

We observed a series of photoelectron images as a function of the pump−probe time-delays and extracted the intensity of the individual components by least-squares fits of the PKEDs to three Lorentzian peaks. The result for pyrazine-D4 is shown in Figure 4 and is compared with the result of H4. Both of the ionization signals from S_1 via the 3s and 3p$_z$ Rydberg states exhibit rapid change during the first 5 ps, which is ascribed to the rotational dephasing of an optically excited S_1 pyrazine.[6,17]

The detailed discussion of the relation between the rotational wave packet dynamics, PKED, and PAD have been described in our previous paper.[6,9,11] Briefly, in the rotational dephasing, an optically prepared molecular axis alignment diminishes to become an isotropic distribution. As the S_1−S_0 transition of pyrazine is a parallel type of a near oblate top, the rotational selection rule is of $\Delta J = 0, \pm 1$ and $\Delta K = 0$. A broad-band femtosecond pump pulse coherently excites the $P(\Delta J = -1)$, $Q(0)$, and $R(+1)$ transitions and creates a superposition of these J states. As the transition is parallel, the figure axis is aligned parallel to the laser polarization at the instant of S_1−S_0 photoexcitation. However, the alignment rapidly diminishes due to the time-evolving phase factors of the J components. The

time-dependent molecular axis distribution in the S_1 state is expressed by

$$P^S(\theta;t) = A^S_{00}(t)Y_{00}(\theta,\phi) + A^S_{20}(t)Y_{20}(\theta,\phi) \propto Y_{00}(\theta,\phi)\left\{1 + \alpha^S_{20}(t)\frac{Y_{20}(\theta,\phi)}{Y_{00}(\theta,\phi)}\right\} \quad (2)$$

where t is the pump−probe delay time, $\alpha^S_{20}(t) = A^S_{20}(t)/A^S_{00}(t)$ is the alignment parameter, $Y_{LM}(\theta,\phi)$ are the spherical harmonics, and θ and ϕ are the polar and azimuthal angles with respect to the space-fixed z axis defined parallel to the polarization of the pump laser.

The time-dependence of the ionization signal shown in Figure 4 originates from the transition from S_1 to the Rydberg states: the transition intensities from the Rydberg states to the ionization continuum do not strongly depend on the axis alignment, because the final states of the transitions have continuum characters where various outgoing partial waves can fulfill the symmetry, energy, and angular momentum requirements. As seen in Figure 4, the transitions from S_1 to 3s and $3p_z$ decrease and increase in the first 5 ps, respectively, indicating that the initial alignment at $t = 0$ is favorable for the former while not for the latter. From this fact, the directions of the transition dipoles in the excitations from S_1 to 3s and $3p_z$ are determined to be parallel and perpendicular to the figure axis of the molecule. As the s orbital has a_g symmetry, the 3s−S_1 transition is readily understood as a parallel transition. The ionization intensity in (1+2′) REMPI through the resonance with the Rydberg state is theoretically expressed in the form of

$$I^S(t) \propto A^S_{00}(t)\{g_1 + g_2\alpha^S_{20}(t)\} \quad (3)$$

where g_1 and g_2 are the constants that vary with the type (parallel and perpendicular) of the Rydberg−S_1 transition and are given elsewhere.[11] The $A^S_{00}(t)$ term is the population in S_1, and it decays exponentially in the present case. For a long time range, both of the photoionization signals from the S_1 state of H4 and D4 gradually diminish due to ISC. Although we have not determined the lifetime of D4 in the present work, it has already been measured by Felker and Zewail by picosecond emission spectroscopy.[18] The lifetime of D4 was 75 ps, much shorter than the 110 ps of H4, due to an increased density of the triplet states.

Close examination of the images shown in Figure 2 reveals the time-dependent photoelectron angular anisotropy. In the cylindrically symmetric system, the LF-PAD resulting from ionization with three photons can be expanded as,[19]

$$I(\theta;t) = \sigma(t)[1 + \beta_2(t)P_2(\cos\theta) + \beta_4(t)P_4(\cos\theta) + \beta_6(t)P_6(\cos\theta)] \quad (4)$$

where $\sigma(t)$ is the integral cross section and $P_L(\cos\theta)$ is a Legendre polynomial. The results obtained for the 3s and $3p_z$ Rydberg states of pyrazine-D4 are shown in Figure 5a with the results of H4 measured under the same experimental conditions. The measurements of D4 and H4 were performed with a 1 month interval after rearrangements of our optical setup. Considering this fact, the agreement between the results of D4 and H4 is surprisingly good, which demonstrates the accuracy of our measurements and the similarity of ionization dynamics between D4 and H4. Both the β_2 and β_4 parameters exhibit rapid change in the first 5 ps due to anisotropy decay, while the variation of β_6 is negligibly small. Because photoionization

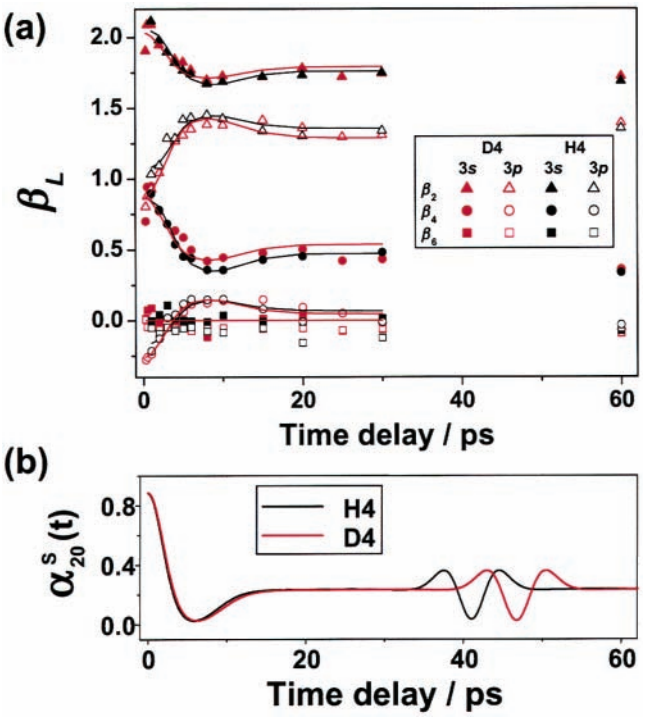

Figure 5. (a) Time-dependent anisotropy parameters, β_2, β_4, and β_6, of the energy selected photoelectron angular distributions in ionization via the singlet 3s and $3p_z$ Rydberg states of pyrazine-D4 and -H4. The solid lines are the least-squares fits to eq 3. (b) Calculated time-dependence of the alignment parameter of the molecular axes, $\alpha^S_{20}(t) = A^S_{20}(t)/A^S_{00}(t)$, in the S_1 state. A rotational temperature of 5 K was assumed in the calculation.

induced by the transition dipole parallel and perpendicular to the top axis provides different partial wave compositions of the outgoing photoelectron, the PAD observed in the laboratory frame (LF-PADs) varies with the relative angle between the top axis and the probe laser polarization. As the Rydberg−S_1 and cation−Rydberg transitions are induced within a femtosecond probe pulse duration, there is no time-evolution of the rotational wave packet in the Rydberg state. The molecular axis distribution in the Rydberg state is then expressed by

$$P^R(t) = A^R_{00}(t)\,Y_{00}(\theta,0) + A^R_{20}(t)\,Y_{20}(\theta,0) + A^R_{40}(t)\,Y_{40}(\theta,0) \quad (5)$$

where

$$\alpha^R_{20}(t) = \frac{A^R_{20}(t)}{A^R_{00}(t)} = \frac{7\sqrt{5}\alpha^S_{20}(t) + f\{7 + 2\sqrt{5}\alpha^S_{20}(t)\}}{7\{\sqrt{5} + f\alpha^S_{20}(t)\}} \quad (6a)$$

and

$$\alpha^R_{40}(t) = \frac{A^R_{40}(t)}{A^R_{00}(t)} = \frac{6f\alpha^S_{20}(t)}{7(\sqrt{5} + f\alpha^S_{20}(t))} \quad (6b)$$

are normalized values of the alignment parameters, and f is a constant factor of 2 or −1 for the parallel or perpendicular Rydberg ← S_1 transition case, respectively. The coefficients $\beta_L(t)$ in eq 4 can be divided into the geometrical (the alignment

TABLE 2: Parameters Determined by the Least-Squares Fits of the Time-Dependent Photoelectron Anisotropy Parameters[a]

	H4 3s	D4 3s	H4 $3p_z$	D4 $3p_z$
a_{000}	$\equiv 1$	$\equiv 1$	$\equiv 1$	$\equiv 1$
a_{200}	0[b]	0[b]	0[b]	0[b]
a_{020}	$0.74 + 0.89a_{420}$	$0.76 - 0.22a_{420}$	$0.65 + 0.33a_{420}$	$0.64 + 0.33a_{420}$
a_{220}	$0.20 - 0.99a_{420}$	$0.17 - 0.12a_{420}$	$-0.19 + 0.75a_{420}$	$-0.29 + 0.75a_{420}$
a_{240}	0.32	0.33	−0.23	−0.27
a_{440}	−0.13	−0.15	−0.15	−0.16
a_{460}	0[b]	0[b]	0[b]	0[b]

[a] Because the basis functions $\alpha^{R}_{K0}(t)$ are not linearly independent, two parameters a_{020} and a_{220} depend on a_{420}. The errors are within 0.03. [b] Assumed.

parameters of the Rydberg state, α^{R}_{K0}) and the dynamical (a_{KL0}) factors:

$$\beta_L(t) = \sqrt{2L+1} \sum_{K=L-2\geq 0}^{L+2} a_{KL0}\alpha^{R}_{K0}(t)/\{a_{000} + a_{200}\alpha^{R}_{20}(t)\} \quad (7)$$

From eqs 6 and 7, it is understood that the photoelectron angular anisotropy ultimately varies with $\alpha^{S}_{20}(t)$. Figure 5a shows the least-squares fit of eq 7 to β_L for ionization via the singlet 3s and $3p_z$ Rydberg states of pyrazine-H4 and -D4. The a_{KL0} values obtained are listed in Table 2. In the analysis, we assumed a_{000}, a_{200}, and a_{460} to be 1, 0, and 0, respectively.

As seen in Figure 5a, the rotational dephasing occurs on the same time-scale as in the H4 case, in agreement with the calculated time-dependent alignment parameter of the molecular axis, $\alpha^{S}_{20}(t)$, in the S_1 state shown in Figure 5b. In the calculations of $\alpha^{S}_{20}(t)$, the rotational temperature was assumed to be 5 K, the rotational constants of $\bar{B}_0 = (A_0 + B_0)/2 = 5.380$ GHz, $C_0 = 2.688$ GHz, and $\bar{B}_1 = (A_1 + B_1)/2 = 5.350$ GHz were used for D4, and $\bar{B}_0 = (A_0 + B_0)/2 = 6.158$ GHz, $C_0 = 3.073$ GHz, and $\bar{B}_1 = (A_1 + B_1)/2 = 6.092$ GHz were used for H4,[20] where the subscripts 0 and 1 denote the constants of S_0 and S_1. Because of the rotational selection rule of $\Delta J = 0, \pm 1$ and $\Delta K = 0$ in the S_1-S_0 transition (under the symmetric top approximation), only the J coherence is created in the S_1 state and the C_1 rotational constant does not affect the results. The anisotropy parameters rapidly increase and decrease in the cases of the $3p_z$ and 3s Rydberg states, respectively. Although these time-dependencies are the same as those of the photoelectron intensities seen in Figure 4, the origins of the time-dependencies are different between the intensity and angular anisotropy. The photoelectron intensity varies with the molecular axis alignment as the bound−bound transition between the S_1 and Rydberg states has the fixed direction in the molecular frame and its angle with respect to the probe laser polarization changes along with the molecular rotation. The transition dipole moment direction in ionization from the Rydberg state to the ionization continuum is unimportant. The PAD is the differential cross section in ionization from the Rydberg state to the continuum. This varies with the molecular axis alignment, as the partial wave composition (such as s, p, d, and f outgoing waves) is different between the ionization through parallel and perpendicular transitions from the Rydberg state to the continuum. (More rigorously, the partial waves must be different for three independent directions of the transition dipole moment in the molecular frame. We approximated here the two directions in the molecular plane are identical to simplify the problem.) The feature seen around 40 ps in Figure 5b is the half revival of the rotational wave packet that we have not attempted to observe in the present work.

Comparing the result on pyrazine-H4 obtained in the present work with the probe wavelength of 393 nm and that with 401 nm,[11] the observed angular anisotropy is higher in the present work. This is certainly an interesting experimental finding; however, it may not be simply regarded as the energy dependence of the continuum wave functions. When the probe laser wavelength varies, so does the energy of the photoelectron scattering wave. However, in our (1+2′) REMPI scheme, the probe laser wavelength also changes the vibrational energy in the Rydberg state from which an electron is ejected. Because of the dual roles of the probe laser wavelength in the present experiment, interpretation of the probe wavelength dependence upon ionization is difficult. In other system, (1+1′) REMPI of NO, we have performed continuum spectroscopy by varying the probe laser wavelength while keeping the same pump laser wavelength.[21]

In summary, we have studied the (1+2′) REMPI of pyrazine-D4 with TR-PEI. The excitation strength from the S_1 0^0 level to the 3s and $3p_z$ Rydberg states is slightly different from that of the H4 case, which is due to smaller Franck−Condon overlap with the highly vibrationally excited levels in 3s and/or the overlap of the probe laser wavelength with the structured absorption spectrum of the $3p_z-S_1$ band. The rotational dephasing time of D4 was quite similar to that of H4, in agreement with the theoretical simulation. The photoelectron angular anisotropies that are surprisingly similar for the D4 and H4 indicate that photoionization dynamics from the 3s and $3p_z$ Rydberg states are essentially identical. No signature was observed of the influence of the superexcited states.

Acknowledgment. This work was financially supported by a Grant-in-Aid from the Ministry of Education, Culture, Sports, Science, and Technology of Japan under contract numbers 13127204, 14204063, and 15002011, and the Japan Science and Technology Agency.

References and Notes

(1) Suzuki, T.; Whitaker, B. J. *Int. Rev. Phys. Chem.* **2001**, *20*, 313. Suzuki, T.; Whitaker, B. J. Photoelectron and photoion imaging with femtosecond pump−probe time clocking. In *Imaging in Molecular Dynamics*; Whitaker, B. J., Ed.; Cambridge University Press: Cambridge, 2003; pp 165. Suzuki, T. Time-resolved photoelectron spectroscopy and imaging. In *Recent Advances in Chemical Reaction Dynamics*; Yang, X., Liu, K., Eds.; World Scientific: Singapore, 2004.

(2) Neumark, D. M. *Annu. Rev. Phys. Chem.* **2001**, *52*, 255. Seideman, T. *Annu. Rev. Phys. Chem.* **2002**, *53*, 41. Stolow, A. *Annu. Rev. Phys. Chem.* **2003**, *54*, 89. Reid, K. L. *Annu. Rev. Phys. Chem.* **2003**, *54*, 397. Stolow, A.; Bragg, A. E.; Neumark, D. M. *Chem. Rev.* **2004**, *104*, 1719.

(3) Pallix, J. B.; Colson, S. D. *Chem. Phys. Lett.* **1985**, *119*, 38. Sekreta, E.; Reilly, J. P. *Chem. Phys. Lett.* **1988**, *149*, 482. Weber, P. M.; Thantu, N. *Chem. Phys. Lett.* **1992**, *197*, 556. Schick, C. P.; Carpenter, S. D.; Weber, P. M. *J. Phys. Chem. A* **1999**, *103*, 10470.

(4) Suzuki, T.; Wang, L.; Kohguchi, H. *J. Chem. Phys.* **1999**, *111*, 4859.

(5) Wang, L.; Kohguchi, H.; Suzuki, T. *Faraday Discuss.* **1999**, *113*, 37.

(6) Tsubouchi, M.; Whitaker, B. J.; Wang, L.; Kohguchi, H.; Suzuki, T. *Phys. Rev. Lett.* **2001**, *86*, 4500.

(7) Matsumoto, Y.; Kim, S. K.; Suzuki, T. *J. Chem. Phys.* **2003**, *119*, 300. Tsubouchi, M.; Suzuki, T. *J. Phys. Chem. A* **2003**, *107*, 10897.
(8) Assion, A.; Baumert, T.; Seyfried, V.; Weiss, V.; Wiedenmann, E.; Gerber, G. *Z. Phys. D: At., Mol. Clusters* **1996**, *36*, 265. Greenblatt, B. J.; Zanni, M. T.; Neumark, D. M. *Chem. Phys. Lett.* **1996**, *258*, 523.
(9) Song, J. K.; Tsubouchi, M.; Suzuki, T. *J. Chem. Phys.* **2001**, *115*, 8810.
(10) Bixon, M.; Jortner, J. *J. Chem. Phys.* **1968**, *48*, 715. Frad, A.; Lahmani, F.; Tramer, A.; Tric, C. *J. Chem. Phys.* **1974**, *60*, 4419. Lahmani, F.; Tramer, A.; Tric, C. *J. Chem. Phys.* **1974**, *60*, 4431.
(11) Tsubouchi, M.; Whitaker, B. J.; Suzuki, T. *J. Phys. Chem. A*, in press.
(12) Eppink, A. T. J. B.; Parker, D. H. *Rev. Sci. Instrum.* **1997**, *68*, 3477.
(13) Chang, B. Y.; Hoetzlein, R. C.; Mueller, J. A.; Geiser, J. D.; Houston, P. L. *Rev. Sci. Instrum.* **1998**, *69*, 1665. Cooper, M. J.; Jackson, P. J.; Rogers, L. J.; Orr-Ewing, A. J.; Whitaker, B. J. *J. Chem. Phys.* **1998**, *109*, 4367. Yonekura, N.; Gebauer, C.; Kohguchi, H.; Suzuki, T. *Rev. Sci. Instrum.* **1999**, *70*, 3265.
(14) Neuhauser, R. G.; Siglow, K.; Neusser, H. J. *J. Chem. Phys.* **1997**, *106*, 896.
(15) Zhu, L.; Johnson, P. *J. Chem. Phys.* **1993**, *99*, 2322.
(16) Fridh, C.; Åsbrink, L.; Jonsson, B. Ö.; Lindholm, E. *Int. J. Mass Spectrom. Ion Phys.* **1972**, *8*, 101.
(17) Myers, A. B.; Hochstrasser, R. M. *J. Chem. Phys.* **1986**, *85*, 6301. Felker, P. M.; Baskin, J. S.; Zewail, A. H. *J. Phys. Chem.* **1986**, *90*, 724.
(18) Felker, P. M.; Zewail, A. H. *Chem. Phys. Lett.* **1986**, *128*, 221.
(19) Yang, C. N. *Phys. Rev.* **1948**, *74*, 764.
(20) Innes, K. K.; Ross, I. G.; Moomaw, W. R. *J. Mol. Spectrosc.* **1988**, *132*, 492.
(21) Tsubouchi, M.; Suzuki, T. Submitted for publication.